Isotopic signatures of precent-day calcite and pyrite in low-temperature crystalline bedrock, Olkiluoto, SW Finland

Seitsamo-Ryynanen, Minja

2022-06

Seitsamo-Ryynanen , M , Karhu , J A , Pitkänen , P & Whitehouse , M 2022 , ' Isotopic signatures of precent-day calcite and pyrite in low-temperature crystalline bedrock, Olkiluoto, SW Finland ' , Applied Geochemistry , vol. 141 , 105308 . https://doi.org/10.1016/j.apgeochem.2022.105308

http://hdl.handle.net/10138/347423
https://doi.org/10.1016/j.apgeochem.2022.105308

Applied Geochemistry 141 (2022) 105308

Contents lists available at ScienceDirect

Applied Geochemistry

journal homepage: www.elsevier.com/locate/apgeochem

Isotopic signatures of precent-day calcite and pyrite in low-temperature crystalline bedrock, Olkiluoto, SW Finland

Minja Seitsamo-Ryynänen [a,*], Juha A. Karhu [a], Petteri Pitkänen [b], Martin Whitehouse [c]

[a] Department of Geosciences and Geography, University of Helsinki, FI-00014, Helsinki, Finland
[b] Posiva Oy Olkiluoto, 27160, Eurajoki, Finland
[c] Department of Geosciences, Swedish Museum of Natural History, 10405, Stockholm, Sweden

ARTICLE INFO

Dr. Zimeng Wang

Keywords:
Calcite
Pyrite
Carbon isotopes
Oxygen isotopes
Sulfur isotopes
Isotope fractionation
Crystalline bedrock
Olkiluoto

ABSTRACT

Geochemical characteristics of precipitated fracture filling calcite and pyrite can provide much useful information about the deep bedrock environment at the time of their deposition. However, it has been difficult to identify fracture coatings precipitated from the present-day groundwater system. The aim of this study was to evaluate the relationship between the coexisting calcite and pyrite, and the groundwater present at the time of precipitation. Here we investigated fine-grained mineral precipitate deposited over a four-year period on the surface of groundwater monitoring equipment inserted into a drillhole at 530 m below sea level, at Olkiluoto, which is the planned site for a final repository of spent nuclear fuel. The experimental setting is also artificial in the sense that the drillholes have possibly affected groundwater circulation and a foreign object has been inserted into the drillhole. Combining the elemental and isotope geochemical composition of the precipitated calcite and pyrite with previously published compositional data on groundwater and evidence for microbial communities on this site, offered a possibility to get new insight of the precipitation and isotope fractionation processes taking place in deep crystalline bedrock. The concentration of the redox sensitive manganese in the precipitate gives supporting evidence for the influx of groundwater from overlying groundwater units. The $\delta^{13}C$ ($n = 13$) and $\delta^{18}O$ ($n = 15$) values of calcite vary from −13.2 to −9.7‰ and from −9.1 to −7.4‰, respectively. Comparison to the respective values in the local groundwater indicated that the precipitated calcite is in near isotopic equilibrium with its environment with respect to carbon and oxygen. The potential ultimate source of the carbon in the DIC and in the precipitate is likely in old fracture calcite coatings. The $\delta^{34}S$ values of pyrite ($n = 9$) show relatively small variation from −5.7 to 8.3‰. This differs greatly from the huge span of $\delta^{34}S$ values from −50 to 80‰ in fracture pyrites reported for the latest calcite fillings at Olkiluoto. The restricted range of $\delta^{34}S$ values is interpreted to result from open system conditions during precipitation, with new dissolved sulfate entering from the large brackish SO_4-type groundwater unit above. The isotopic fractionation of sulfur between dissolved sulfate and sulfide is estimated to be 25 ± 10‰, which is in agreement with the results reported in laboratory experiments for bacterial sulfate reduction.

1. Introduction

In deep crystalline bedrock, minerals precipitate from groundwater residing in fracture networks. Calcite and pyrite are typical minerals formed in water conducting fractures (e.g. Blyth et al., 2000; Gehör et al., 2002; Tullborg et al., 2008). These minerals precipitate from water flowing in fractures and sensitively react to their composition reflects changes in water composition, and therefore their geochemical characteristics can provide much useful information about the deep bedrock environment at the time of their deposition. Especially, carbon and oxygen isotope ratios in calcite and sulfur isotope ratios in pyrite have turned out to be useful geochemical tools in investigating the paleohydrogeological evolution of the conductive fracture networks (e.g. Sahlstedt et al., 2010; Smellie et al., 2014; Drake et al., 2009; Tullborg et al., 1999; Blyth et al., 2000).

Calcite and pyrite are known to precipitate under a wide range of conditions, from high-temperature hydrothermal environment to low-temperature groundwater circulation (e.g. Iwatsuki et al., 2002; Blyth et al., 2004, 2009; Sahlstedt et al., 2010, 2013, 2016; Drake et al., 2012; Drake and Tullborg, 2009). Several studies have been targeted to

* Corresponding author.
E-mail address: minja.seitsamo-ryynanen@helsinki.fi (M. Seitsamo-Ryynänen).

https://doi.org/10.1016/j.apgeochem.2022.105308
Received 22 December 2021; Received in revised form 13 April 2022; Accepted 20 April 2022
Available online 26 April 2022

identify and investigate the most recent fracture mineral precipitation events (Gehör et al., 2002; Sahlstedt et al., 2010, 2016; Drake et al., 2015b, 2017). Although much useful information has been obtained, it has been difficult to conclusively identify fracture coatings precipitated from the present-day groundwater system (Sahlstedt et al., 2010; Drake and Tullborg, 2009; Drake et al., 2018b).

Water conducting fractures in deep crystalline bedrock are without exceptions saturated or oversaturated with respect to calcite (Allard et al., 1983; Pitkänen et al., 2004). It is conceivable that small disturbances in the groundwater system may lead to calcite precipitation. Evidence for recent calcite deposition may be provided by the apparent isotopic equilibrium of oxygen and carbon in the mineral with the present-day groundwater. Especially, for oxygen isotope ratios, evidence for equilibrium conditions has been provided by many studies (Sahlstedt et al., 2010; Drake and Tullborg, 2009; Tullborg et al., 2008; Drake et al., 2018a). The contents of dissolved inorganic carbon (DIC) in deep crystalline bedrock are generally low due to high calcium contents in saline groundwaters, and only a few measurements of $\delta^{13}C$ values in DIC for comparison to those in fracture wall calcites have been reported. Based on these analyses, the $\delta^{13}C$ values of the latest calcite fillings appear to be commonly in disequilibrium with the DIC in the modern local groundwater (Sahlstedt et al., 2010). However, the groundwater types may have changed, and the groundwaters coexisting with the latest calcite precipitates at the time of their formation may have been different from those in the present-day fracture system. Therefore, additional data are needed from coexisting components and phases in the groundwater system.

Deep anoxic groundwaters in crystalline bedrock sustain microbial life capable of bacterial sulfate reduction (BSR). Indications for active BSR is provided by the abundant existence of sulfate reducing bacteria in deep groundwaters (Pedersen et al., 2008; Halbeck and Pedersen et al., 2008). In the presence of organic carbon substrate or hydrogen as the electron donor, these bacteria are able to use sulfate as the electron acceptor. As a result of BSR, dissolved sulfide is formed in groundwater. Because deep anoxic groundwaters generally contain dissolved iron (Pitkänen et al., 2004; Laaksoharju et al., 2008), sulfide is subsequently precipitated as metastable iron mono sulfide (FeS), which is transformed into insoluble pyrite (FeS_2) by reaction with dissolved H_2S or intermediate oxidation state sulfur species (Morse et al., 1987; Rickard and Luther, 2007). In laboratory settings, replacement processes have been observed to proceed rapidly within days (Schoonen and Barnes 1991; Rickard 1997). However, field studies indicate that the complex mechanism of either process are significantly delayed in natural environments (Kraal et al., 2013). Elevated dissolved sulfide contents have often been observed in water samples from the present-day fracture network in deep crystalline bedrock (Pitkänen et al., 2004; Posiva, 2013; Drake et al., 2013), providing strong evidence for ongoing BSR. Knowing the abundance of dissolved Fe and the presence of sulfate reducing bacteria, present-day precipitation of pyrite on the fracture walls is highly probable, although difficult to prove in natural fracture environments.

In a low temperature environment, the sulfur isotope ratios of pyrite are mainly determined by fractionations associated with microbial redox reactions in BSR (e.g. Canfield, 2001). The light ^{32}S isotope is enriched in the product sulfide relative to the composition of the dissolved sulfate. In laboratory cultures, the fractionations between sulfate and sulfide have been observed to reach about 45‰ (Harrison and Thode, 1958; Kaplan and Rittenberg, 1964; Chambers and Trudinger, 1979; Habicht et al., 1998; Detmers et al., 2001), and up to about 70‰ (Canfield et al., 2010; Sim et al., 2011). In natural systems, the largest apparent sulfur isotope fractionations between sulfide and sulfate have been observed to reach 71‰ (Drake et al., 2015a, 2018c; Wortmann et al., 2001). These high isotopic separation values cannot be easily explained by BSR alone and have been possibly enhanced by redox cycling and disproportionation reactions (Canfield and Thamdrup, 1994; Habicht and Canfield, 1997, 2001; Habicht et al., 1998). However, due to problems in the identification of coexisting sulfate-sulfide pairs, it has been difficult to get direct evidence of the magnitude of sulfur isotope fractionation in the present-day fracture network.

Instead of attempting to identify present-day fracture coatings, it is possible to use an artificial setting, where a foreign object has been placed in contact with a water conducting fracture and later recovered for inspection. Any precipitate on the surface of the object is definitively formed in the presence of modern groundwater in the conducting fracture. Using this kind of an approach, Drake et al. (2015a) investigated the environmental conditions leading to pyrite precipitation in crystalline bedrock fractures at the Äspö site in Sweden, and Drake et al. (2018a) studied the isotopic composition of calcite and the distribution of trace elements between calcite and water under low temperature conditions. The setting is not natural, as drillhole environment deviates from undisturbed fracture system, and drillhole instrumentation may add to that deviation. It is possible that, the precipitation may have been caused or affected by disturbances of the system. Nevertheless, this experimental setting allows the evaluation of geochemical and isotope geochemical relationships between the coexisting minerals and groundwaters in the existing fracture network.

In this study we investigated brownish, fine-grained material observed to have been deposited on the surface of an acid-resisting stainless steel groundwater monitoring equipment inserted into drillhole OL-KR46 in crystalline bedrock, at a depth of 530 mbsl, at Olkiluoto, southwestern Finland. The instrumentation was recovered in 2017 after being in contact with local fracture water since 2013. In a closer inspection, the material on the surface of the instrumentation turned out to comprise mostly of micrometer sized calcite and some microcrystalline pyrite crystals. The present-day hydrogeochemical environment and groundwater formation at Olkiluoto is well known due to extensive investigations for planning a nuclear waste repository site (Posiva, 2013; Pitkänen et al., 2004). However, direct observations of mineral-water pairs are needed to better understand these geochemical systems and the geochemical changes resulting from tunneling and repository construction. Specifically, copper canisters used to store spent nuclear fuel can be affected by sulfide enhanced corrosion, and the isotopic composition of sulfur in pyrite may provide important insight into the geochemical characteristics of the sulfur system in deep crystalline bedrock. The aim is to evaluate the relationship between the coexisting drillhole precipitate and the groundwater present at the time of precipitation, and to better understand the isotope fractionation processes taking place in deep crystalline bedrock.

2. Geological and hydrogeochemical setting

Olkiluoto is an island on the western coast of Finland, located ca. 10 km north of the city of Rauma (Fig. 1). The bedrock of the Olkiluoto area belongs to the Paleoproterozoic rock units of southwestern Finland. The main rock types on the island are gneisses and migmatitic gneisses (Aaltonen et al., 2016; Kärki and Paulamäki, 2006). Granitic intrusions associated with migmatites were emplaced during the Svecofennian orogeny (Suominen et al., 1997; Veräjämäki 1998). A detailed description of the Olkiluoto bedrock can be found in Aaltonen et al. (2016) and Kärki and Paulamäki (2006).

Based on chemical and isotopic characteristics, groundwaters at Olkiluoto can be divided into distinct water types (Fig. 1), occurring as roughly horizontally stratified water bodies (Pitkänen et al., 2004; Posiva, 2013). Hydraulically active zones display deviations from horizontal layers. The upper 100 m of the bedrock is dominated by HCO_3^--type groundwater with salinity rising from fresh to brackish with increasing depth. This groundwater type has been interpreted as a mixture of meteoric water, Baltic Sea water and fresh water derived from a man-made Korvensuo reservoir in the middle of the island. Water in this uppermost layer is relatively young and has formed after the island emerged from the Baltic Sea as a result of post-glacial uplift approximately 2500–3000 yrs ago (Posiva, 2013). Brackish sulfate-type waters, with SO_4^{2-}-concentrations ranging from 123 to 510 mg/L (Posiva,

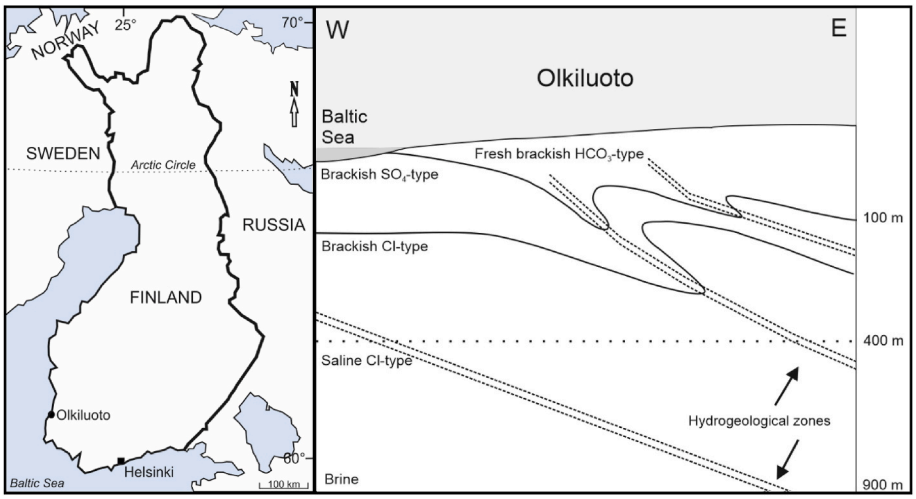

Fig. 1. Hydrogeological setting. A schematic illustration of the groundwater types at Olkiluoto (modified after Posiva, 2013). Hydrogeological zones with higher water conductivity disturb the otherwise horizontal layering of the geochemical groundwater types.

2013), dominate groundwater at the depth of 100–300 m. This water type has been interpreted to have been infiltrated during the Littorina Sea stage of the Baltic Sea, beginning at 8500 yrs ago (Björk, 2008). Locally, there is evidence of mixing of sulfate-type waters with older subglacial and glacial melt waters (Posiva, 2013). Below the depth of 300 m, the groundwaters are dominated by brackish and saline Cl-type waters, representing diluted ancient brines. A detailed description of the composition and evolution of groundwaters at the Olkiluoto site is found in Pitkänen et al. (2004) and Posiva (2013).

The construction of a deep nuclear waste repository ONKALO has caused deviations in the hydrogeological conditions from the baseline, especially in the proximity of major hydraulically active zones. These include a drawdown of sulfate-rich groundwater, evidenced by elevated sulfate content in drillholes observed locally nearly 300 m below the lower boundary of the sulfate-rich layer at 300 m (Posiva, 2013). The study site has a complex geological history and the paleohydrological evolution of the deep groundwater system has been extensively studied using fracture minerals, especially including calcite and pyrite (e.g. Blyth et al., 2000; Gehör et al., 2002; Sahlstedt et al., 2010, 2013, 2016).

The evolution of the geochemical composition and the microbial activity of fracture water has been monitored (Bell et al., 2018, 2020). Previous studies have demonstrated that groundwater in the targeted fracture system in drillcore OL-KR46 at 530 mbsl contains high concentrations of dissolved sulfide from 0.5 to 1.5 mM (Lamminmäki et al., 2017a; Bell et al., 2018), and 0.6–5.8 mM sulfate with $\delta^{34}S_{SO4}$ ranging from +23 to +35‰ (VCDT, Lamminmäki et al., 2017b; Bell et al., 2018). The DIC contents are very low and have been reported to range from below detection limit up to 4.6 mg/L, with $\delta^{13}C_{DIC} \sim -15‰$ (Bell et al., 2018). Fracture water contains about 1.5 mM methane, with $\delta^{13}C_{CH4} \sim -32‰$ (Bell et al., 2018). The DOC contents have been reported to range from 18 to 73 mg/L (Lamminmäki et al., 2017b; Bell et al., 2018) with $\delta^{13}C_{DOC} \sim -21‰$ (Tuomi et al., 2020). A recent study indicates that 65% of the total carbon mass of DOC in this fracture water system is contributed by acetate (Bell et al., 2018).

The high concentration of dissolved SO_4 in drillhole OL-KR46 at 530 mbsl is unusual and has not been observed in earlier studies at this depth. It has been concluded that drilling and tunnel construction operations have affected the natural groundwater conditions in the fracture network, causing an inflow of sulfate-rich groundwater to the research site (Posiva, 2013). As a result, dissolved sulfate has introduced an abundant electron acceptor for microbial metabolic processes and sulfate reduction has commenced. In a metaproteogenomic study of groundwater samples from this site, Bell et al. (2018) concluded that sulfate-reducing bacteria were the most abundant metabolic group, with indications of sulfate reduction being an active metabolic process. Geogenic hydrogen and acetate produced by acetogenic bacteria were inferred to have been the sources of electrons and carbon for BSR (Bell et al., 2018).

3. Materials and methods

3.1. Sampling

Fracture water in drillhole OL-KR46, at 530 m below sea level (mbsl) has been sampled regularly since 2013. The depth range of 528.2–531.5 mbsl was isolated with inflatable double packers in December 2013 containing a low transmissivity fracture at 530.6 mbsl. The double packers were connected to each other with a corrosion resistant stainless steel rod. Hydrogeochemical data for the water samples collected from the isolated section of the drillhole containing a water conducting fracture have been reported by Lamminmäki et al. (2017a, b, c) and Bell et al. (2020). The drillhole instrumentation was extracted in March 2017. Mineral precipitate was discovered to be present on the plastic tubing as well as on the steel rod of the drillhole equipment that did not show visible corrosion. The precipitate was scraped off for further analysis using a steel blade and stored in a closed plastic bottle.

The precipitate grains were composed mostly of small calcite crystals and minor amounts of microcrystalline iron sulfides. Calcite and sulfide grains were hand-picked under a stereomicroscope and mounted on epoxy. Epoxy buttons were then studied using a scanning electron microscope (SEM) equipped with an energy dispersive spectrometry (EDS) detector in a low-vacuum mode. The same epoxy buttons were used for spot analysis of the isotopic composition of carbon and oxygen in calcite and that of sulfur in pyrite.

3.2. Secondary ion mass spectrometry

Carbon and oxygen, and sulfur isotope analyses were performed using a CAMECA IMS 1280 large geometry secondary ion mass spectrometer (SIMS) at the NordSIM facility in Stockholm, Sweden. Analytical settings are described briefly below.

For $^{13}C/^{12}C$, $^{18}O/^{16}O$ and $^{34}S/^{32}S$ ratios, the samples were sputtered using a critically focused $^{133}Cs^{+}$ primary beam with 20 kV impact. A low-energy/normal-incidence electron gun was used for charge compensation. Each analysis consisted of an initial pre-sputter to remove the gold coating; the secondary beam being centered into the field of aperture. All pre-sputter, beam centering and data acquisition steps were performed in automated sequences by the run definition, and

at the beginning of the session the magnetic field was locked using an NMR field sensor. The vacuum in the sample chamber was maintained at $<2 \times 10^{-8}$ mbar.

A total of 15 calcite samples were analyzed for $\delta^{13}C$ and $\delta^{18}O$. Analysis points were targeted at a sufficient distance from grain boundaries. The primary beam was homogenized using a 10 μm raster, resulting in a ~15 μm analytical spot. The initial 50-s pre-sputter raster was 20 μm. Oxygen isotopes were measured on 2 F detectors at a mass resolution of 2500. To resolve ^{13}C from $^{12}C^{1}H$, the secondary ion signals of ^{12}C and ^{13}C were measured in a multicollector mode using a Faraday detector for ^{12}C and an ion counting electron multiplier for ^{13}C at a mass resolution of 4000. The isotope data was corrected for instrumental mass fractionation using matrix-matched standards mounted together with the sample mount and analyzed after every five to six sample analyses. The standard used for calcite was S0161 cc carbon and oxygen isotope standard. After propagating the within-run and external uncertainties from standard measurements, the typical precision of a single $\delta^{13}C$ and $\delta^{18}O$ were ±0.37‰ and ±0.16‰, respectively.

For the sulfur isotope ratio measurements, the primary beam produced a ~15 μm analytical spot, and the initial 60-s pre-sputter raster was 20 μm. Secondary ion signals were detected simultaneously using 2 F cups with a common mass resolution of 4860. A total of 22 sulfide samples were analyzed. The pyrite standard used was S0302A.

Because the size of the pyrite grain accumulations on the sample surface was similar or smaller than the analytical spot of the instrument, the precision was estimated by a beam-planking method (Fig. 2). The $\delta^{34}S$ value of the S0302A pyrite standard was measured repeatedly by diverting a variable fraction of the primary beam from the sample surface, that way reducing the count rate fraction of the secondary beam. The $\delta^{34}S$ deviation for a count rate fraction from 1 to 0.2 varied from 0.03 to 0.05‰, well within the normal precision for sulfur analyses conducted by the SIMS instrument (±0.2‰). With the count rate fraction 0.1, the $\delta^{34}S$ deviation was higher, but the precision remained <1.0‰. All analyses with a count rate fraction exceeding 0.1 were accepted, and the precision of a single $\delta^{34}S$ value is therefore estimated to be < 1.0‰.

The isotope results of oxygen and carbon in calcite and sulfur in pyrite are reported in per mil (‰) against the Vienna Pee Dee Belemnite (VPDB) and Vienna Cañon Diablo Troilite (VCTD) standards, respectively, using the δ-notation defined as:

$$\delta_x = \left[\frac{R_{sample}}{R_{standard}} - 1\right] 1000 \quad \text{(Eq. 1)}$$

where R is the $^{13}C/^{12}C$, $^{18}O/^{16}O$ or $^{34}S/^{32}S$ ratio, and the standard is Vienna Peedee Belemnite (VPDB) for $^{13}C/^{12}C$ and $^{18}O/^{16}O$, and Vienna-Canyon Diablo Troilite (VCDT) for $^{34}S/^{32}S$. The typical precision was ±0.30‰ for $\delta^{13}C$ and ±0.14‰ for $\delta^{18}O$ at 1σ level, after considering the within-run and external uncertainties from standard measurements.

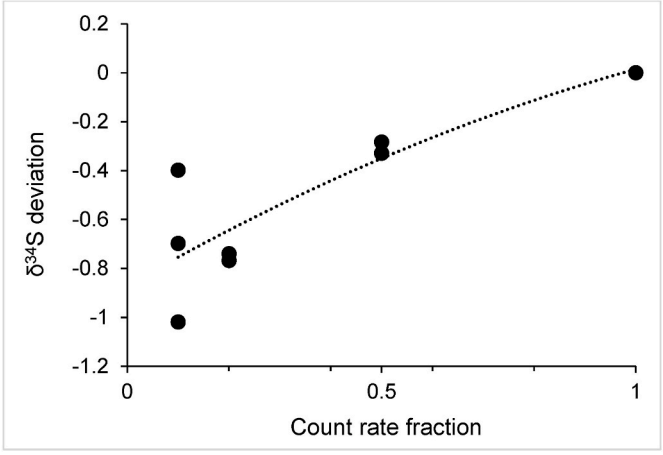

Fig. 2. The $\delta^{34}S$ deviation of a count rate fraction using beam-planking method. The precision of a single $\delta^{34}S$ value was estimated to be < 1.0‰ for count rates as low as 0.1.

The analytical settings closely follow those previously reported by Kamber and Whitehouse (2007), Drake et al. (2013), Drake et al. (2015b), and Sahlstedt et al. (2016).

3.3. Electron probe microanalysis and ICP-MS

The contents of Ca, Mg, Mn, Fe and Zn in calcite were determined by wavelength-dispersive electron probe microanalysis (EPMA). Analysis was conducted using a JEOL JXA-8600 Superprobe instrument upgraded with the SAMx analytical software package and PointElectornic SAMx hardware at the Department of Geosciences and Geography, University of Helsinki, Finland. Mineral identification was aided by qualitative measurements with energy dispersive spectrometry (EDS), using 15 kV acceleration voltage and 1 nA beam current. The quantitative WDS measurements were performed using a 10 μm defocused beam at 15 kV acceleration voltage and a beam current of 10 nA. Standard materials were dolomite for Mg, calcite for Ca, rhodonite for Mn, almandine for Fe, and sphalerite for Zn. The measurement time was 20 s at the peak position and 10 s at each background position. The accuracy of the EPMA analyses determined by measuring standard materials as unknowns was about 2% for major elements and 5% for minor elements. Each selected analysis spot (n = 10) was within 20–30 μm from the respective isotope analysis spot.

A subsample of the precipitate was dissolved to 5% nitric acid and analyzed for the contents of S, Fe and U by an Agilent 7500ce/cx ICP-MS instrument at the Department of Geosciences and Geography, University of Helsinki. The analytical error of the analyses was estimated to be 1–5% of the measured value.

4. Results

Under optical inspection, the precipitate crusts included two distinct types of carbonate grain accumulations. The first type consisted of 50–100 μm calcite crystals and other precipitated materials, such as iron sulfides, on top of the calcite. Euhedral calcite grains showed rounding of the edges, indicating partial dissolution (Fig. 3a). The second type of carbonate grain accumulation consisted of smaller, 20–50 μm, euhedral carbonate crystals with sharp edges (Fig. 3b). This type of carbonate crystals also contained iron sulfides and other precipitated materials. Carbonate was confirmed to be calcite by X-ray diffraction (XRD). Accumulations formed on different surface materials were not treated separately during sample collection.

According to EPMA, the calcite in the precipitate contains 0.8–1.1 wt % Mn and 0.5–0.7 wt% Mg (Appendix 1). In addition to carbonate, the precipitate contains Al-rich silicate flakes as well as <5 μm microcrystalline pyrite which tends to form groups of adjacent grains. The ICP-MS determination yielded 0.49 wt% S and 0.49 wt% Fe, but the XRD did not show any evidence for crystalline sulfide phases in the bulk sample, possibly due to the low contents of sulfide. Mineral grains with a general composition of FeS_2 were however detected and analyzed by EPMA-WDS. Based on optical properties, the mineral is pyrite. Iron monosulfides were not observed.

Polished epoxy grain mounts prepared for the isotopic analyses demonstrated tiny pyrite grains between large calcite crystals. The $\delta^{13}C$ and $\delta^{18}O$ values of calcite ranged from −13.2 to −9.7‰ and from −9.1 to −7.4‰, respectively (Appendix 2). The two morphological types of carbonate showed no difference in their isotopic composition. The $\delta^{34}S$ values of pyrite ranged from −5.7 to 8.3‰ (Appendix 2). The identification of pyrite does not necessarily exclude the presence of iron monosulfide. The fractionation of sulfur isotopes between FeS and FeS_2 is negligible (Wilkin and Barnes, 1996), and the $\delta^{34}S$ values of pyrite are therefore also representative of FeS.

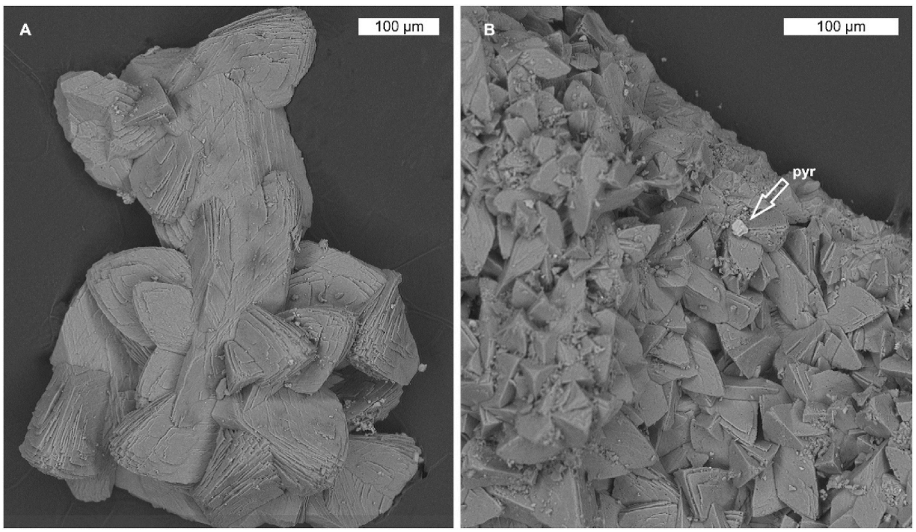

Fig. 3. Backscattered electron (BSE) images of: (a) large euhedral calcite crystals with slightly rounded edges, (b) smaller euhedral calcite crystals and cubic pyrite (pyr).

5. Discussion

In order to understand calcite and pyrite precipitation processes in deep crystalline low-temperature setting, we need to know geochemical characterization of groundwater at the precipitation depth, and potential sources of carbon and sulfur. In this study, we aimed to answer these questions by combining elemental and isotope geochemistry of calcite and pyrite with previously published data on groundwater and microbial conditions at the study site.

5.1. Redox-sensitive elements in the precipitate

The concentration of the redox-sensitive element manganese in the precipitate can provide information about changes in the oxidation potential and give supporting evidence for the influx of groundwater from overlying groundwater units. In general, high contents of Mn has been observed to be characteristic for fracture minerals at a shallow depth, whereas lower contents occur at deeper levels (Fig. 4).

In the precipitate, the average MnO content of calcite is 1.16% (Fig. 4). Typically, Mn content in fracture filling calcite shows large variation and clear decrease with increasing depth (Drake and Tullborg, 2009; Sahlstedt et al., 2010). In earlier studies, a MnO content >1 wt% in late-stage calcite filling has only been encountered at a depth of <400 m (Sahlstedt et al., 2010; Sahlstedt and Karhu, 2016; Posiva, 2013). In this respect, the Mn content of the calcite precipitate differs greatly from the baseline conditions at the depth of 500–600 m (Fig. 4).

Considering the high contents of the redox-sensitive elements Mn in the precipitate, its chemical composition is not typical for fracture fillings formed at depths of >500 m, but it instead resembles fracture coatings formed closer to the bedrock surface, where manganese reduction provides Mn^{2+} to be incorporated in calcite. This observation supports the earlier conclusion that artificial drillhole settings have caused drawdown of groundwater from overlaying groundwater units with high contents of dissolved SO_4 and Mn.

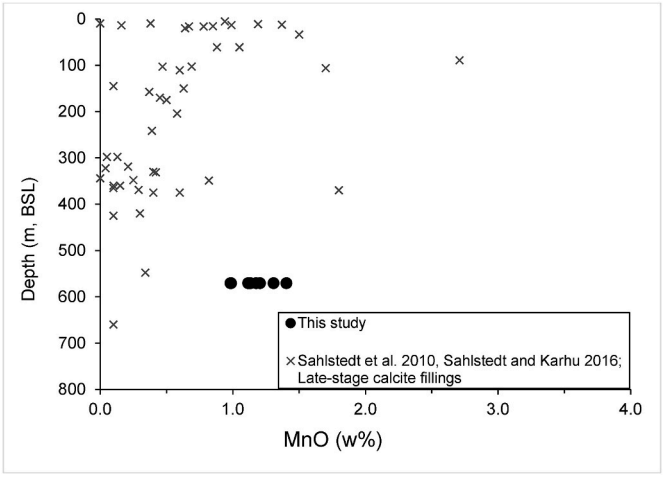

Fig. 4. Concentration of MnO in calcite precipitated on top of instruments compared to published data of MnO contents in late-stage fracture calcite at Olkiluoto.

5.2. $\delta^{18}O$ and $\delta^{13}C$ values of calcite

The $\delta^{18}O$ values of calcite show relatively little variation from −9.1 to −7.4‰ (Fig. 5). This is expected based on the observed small range of $\delta^{18}O$ values of water from −10.2 to −8.2‰ (VSMOW) and the nearly constant temperature of 12.6 °C in fracture water during the 5-year period (Lamminmäki et al., 2017a, b, c; Bell et al., 2020). Applying the fractionation factor of O'Neil et al. (1969), the $\delta^{18}O$ values are in the range of calcite precipitated in equilibrium with the present-day

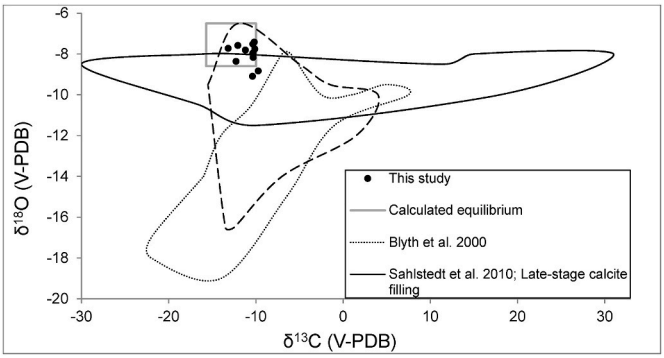

Fig. 5. $\delta^{13}C$ and $\delta^{18}O$ values of calcite in the precipitate compared to reported values in fracture filling calcite at Olkiluoto. Analytical errors are smaller than the size of the symbols. Boxed area indicates the calculated C and O isotopic composition of calcite precipitating in equilibrium with the present-day waters in the drillhole.

groundwater enclosing the instrumentation at the ambient temperature of 12–13 °C. Near isotopic equilibrium was reported also by Drake et al. (2018a) in calcite precipitated over a 17-year period in contact with monitored fracture water.

The $\delta^{18}O$ values of the calcite in the precipitate are among the highest values reported for fracture filling calcite at Olkiluoto (Fig. 5). This can be understood in terms of differences in the precipitation temperature and the isotopic composition of oxygen in the fracture water. Previous studies indicates that the older fracture calcites have been formed in hydrothermal conditions at elevated temperatures, with a lower fractionation factor of oxygen between calcite and water (Blyth et al., 2000; Sahlstedt et al., 2010).

The $\delta^{13}C$ values of precipitated calcite fall in a relatively narrow range from −13.2 to −9.7‰ (Fig. 5). Using the fractionation factors by Romanek et al. (1992) and Zhang et al. (1995) and the speciation of carbon among the different DIC species, the carbon isotope fractionation between calcite and DIC can be calculated to be relatively small ($1000\ln\alpha \sim 1.5‰$) for a solution at a pH of 8–9 and a temperature of 12.6 °C. The contents of DIC in drillhole OL-KR46 at 530 mbsl are very low and only a few determinations of the isotopic composition of carbon in DIC have been published. The $\delta^{13}C$ values of DIC have been reported to vary from −16.9 to −14.2‰ (Bell et al., 2018). Accordingly, the precipitated calcite appears to be in near isotopic equilibrium with its environment also with respect to carbon.

The small variability in carbon isotope ratios in calcite is completely different from the extreme variability in the $\delta^{13}C$ values of the latest fracture calcite fillings at Olkiluoto, with values ranging from −30 to 30‰ (Fig. 5). The highly positive and the highly negative $\delta^{13}C$ values have been addressed to methanogenic and methanotrophic processes, respectively (Sahlstedt et al., 2010). Clearly, the carbon isotope ratios of DIC in the investigated precipitation environment do not show any evidence of methane-related processes. This is surprising, as the groundwater at the site has been measured to contain 1–1.8 mM of CH_4 with a $\delta^{13}C_{CH4}$ value of ~ −32‰ and active methanogenic microbial communities have been identified at the site of the investigation (Bell et al., 2018).

Fracture calcites in the Olkiluoto bedrock have a huge variability in their $\delta^{13}C$ values from −50 to 40‰, but a large majority of them have $\delta^{13}C$ values between −15 and −5‰ with a strong mode in values between −15 and −10‰ (Fig. 6). This range also includes all $\delta^{13}C$ values of the precipitated calcite investigated in this study. These results strongly suggest that dissolution of old fracture calcite coatings is a potential ultimate source of carbon for the DIC and the new precipitate.

DOC is an important dissolved carbon component in drillhole OL-KR46 at 530 mbsl, having concentrations clearly higher than those of DIC. DOC has been determined to consist predominantly of acetate (Bell et al., 2018). Bell et al. (2018) were also able demonstrate the presence of acetogenic bacteria *Acetobacterium* at the site, suggesting that acetate may have been derived autotrophically as a metabolic product in the acetyl coenzyme A (Acetyl- CoA) pathway or by fermentation.

The $\delta^{13}C$ of the DOC at the research site has been reported to be −21.7‰ (Tuomi et al., 2020). Because acetate is the dominant component of DOC, this isotope value may also closely approximate that of carbon in acetate. In laboratory experiments, the Acetyl-CoA pathway has been observed to strongly prefer ^{12}C in the product acetate, with an average fractionation of about 57‰ from the substrate, whereas fermentation has been observed to cause almost no fractionation for the isotopic composition of carbon (Blaser et al., 2013). Therefore, the relatively high $\delta^{13}C$ value of the DOC gives indications that acetate formation could be mostly related to fermentation. Carbon isotope data specifically from acetate are needed to provide better constraints for the origin of acetate and to better understand the complex carbon isotope system.

Partly, the dissolution of the old fracture filling calcite could have occurred at the depth of the instrumentation. However, it is likely that drawdown of groundwaters from the overlaying water units has also contributed as a carbon source for the calcite precipitate.

5.3. $\delta^{34}S$ values of pyrite

The $\delta^{34}S$ values of pyrite in the precipitate have relatively little variation from −5.7 to 8.3‰ (Fig. 7). This is in strong contrast to the huge span of the published $\delta^{34}S$ values from −50 to 80‰ in fracture pyrites associated with the latest calcite fillings at Olkiluoto (Fig. 7). A similar extensive span of $\delta^{34}S$ values of more than 100‰ was observed by Drake et al. (2015a), who studied calcite and pyrite precipitates formed on top of drillhole instruments at Äspö, Sweden.

Dissolved sulfate in the brackish SO_4 -type groundwater (Fig. 1) is thought to have been originally derived from the inflow of brackish water from the former Littorina Sea stage of the Baltic Sea basin (Posiva, 2013). The $\delta^{34}S$ values of sulfate in this groundwater type range from 22 to 38‰ (Posiva, 2013). These $\delta^{34}S$ values are distinctively higher than those in sulfate of the present-day Baltic Sea water, with a marine $\delta^{34}S$

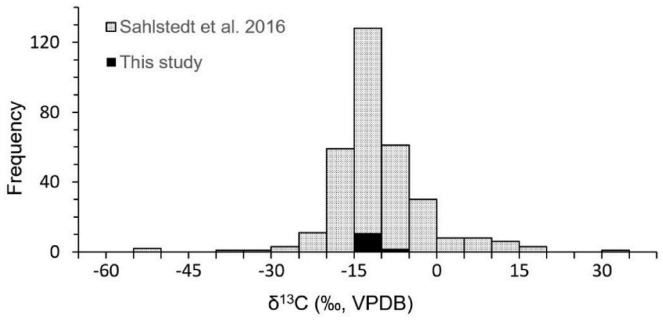

Fig. 6. Histogram showing the distribution of the $\delta^{13}C$ values of calcite precipitated on the drillcore equipment compared to the reported $\delta^{13}C$ values of fracture filling calcite in the Olkiluoto bedrock.

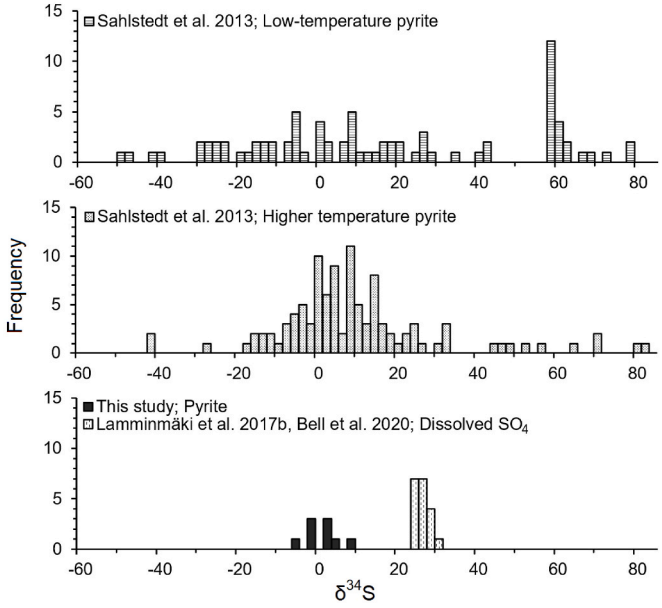

Fig. 7. Histogram showing the distributions of $\delta^{34}S$ values of pyrite precipitated on the drillcore equipment compared to the reported $\delta^{34}S$ values of fracture pyrite in the Olkiluoto bedrock. Open columns represent published $\delta^{34}S$ values of fracture water sulfate in OL-KR46 at 530 mbsl (Lamminmäki et al., 2017b; Bell et al., 2020). Temperature classification based on the associated calcite precipitates and the $\delta^{34}S$ data of fracture filling pyrite at Olkiluoto is according to Sahlstedt et al. (2013). Low temperature represent precipitation at a <50 °C, and higher temperature represent temperature range of 50–90 °C and older hydrothermal events.

value of ~ +20‰. The increase has been addressed to microbial SO_4 reduction during the infiltration of the seawater through the bottom sediments (Posiva, 2013), which has preferentially removed ^{32}S as sulfide from the sulfate pool. The $\delta^{34}S$ values of dissolved sulfate in drillhole OL-KR46 at 530 mbsl vary from +23 to +35‰, which are similar to values measured for sulfate in the brackish SO_4 -type waters (Posiva, 2013).

The high contents of dissolve sulfide in fracture water at the site of the precipitation and the presence of pyrite in the precipitate indicate active BSR in groundwater. The conclusion is in line with the observation of sulfate-reducing bacteria being the most abundant metabolic group in fracture water at the site (Bell et al., 2018).

Several variables have been observed to affect the fractionation of sulfur between sulfate and sulfide in BSR. These include the availability of dissolved sulfate (Zaback et al., 1993; Canfield, 2001; Habicht et al., 2002), which has been observed to reduce fractionation in experimental settings containing less than ca. 1 mM sulfate (Harrison and Thode, 1958; Habicht et al., 2002). In addition, the rate of BSR and the type of bacterial communities have been noted to affect sulfur isotope separation (Detmers et al., 2001; Canfield, 2001; Habicht and Canfield, 2001; Canfield et al., 2010).

The $\delta^{34}S$ determinations from coexisting dissolved sulfate and precipitated pyrite can be utilized to estimate sulfur isotope fractionation in BSR. Using the published $\delta^{34}S$ values of dissolved sulfate and the $\delta^{34}S$ values of pyrite (this study), the fractionation can be estimated to be 25 ± 10‰ (2sd). The calculated fractionation is similar to that produced by BSR in laboratory experiments between dissolved sulfate and sulfide. In these experiments, most fractionation estimates according to Johnston et al. (2007) cluster around 25‰ ± 10‰. The concentration of dissolved sulfate in fracture water is high, varying from 0.6 to 6 mmol/L, and the fractionation is not expected to have been restricted by low contents of sulfate (Habicht et al., 2002).

The huge variability of the $\delta^{34}S$ values observed in the natural fracture system at Olkiluoto by Sahlstedt et al. (2013) and in Sweden by Drake et al. (2013; 2018c) has been explained in terms of fractionation related to BSR under closed or partially closed system conditions. When the availability of dissolved SO_4 is limited, or the rates of BSR are very high relative to SO_4 inflow (Gomes and Hurtgen 2013), the $\delta^{34}S$ values of the remaining SO_4 will increase progressively due to the removal of sulfide depleted in ^{34}S in a Rayleigh-type process.

Drake et al. (2015a) investigated pyrite precipitation on drillcore equipment at Äspo, Sweden. Their results suggested a very large fractionation of 71‰ between the $\delta^{34}S$ values of sulfate and sulfide. In addition, they noticed that the sulfur isotope ratios increased up to 60‰ in single crystals from core to rim, indicating precipitation in closed-system conditions, where the sulfate pool is consumed by BSR.

There are two fundamental differences in the sulfur isotope data published by Drake et al. (2015a) from the data reported in this study. Firstly, the pyrite precipitates at Olkiluoto suggest a relatively small fractionation in BSR between sulfate and sulfide of 25 ± 10‰. Secondly, the $\delta^{34}S$ pattern at Olkiluoto does not provide any evidence that the reservoir of dissolved sulfate would have been exhausted by BSR. Whereas the precipitation system at Äspo represents closed-system conditions, at Olkiluoto the local system has been open during precipitation, with new dissolved sulfate introduced from the brackish SO4-type groundwater unit above.

The large difference in the estimates of the sulfur isotope fractionation between sulfate and sulfide is more difficult to understand. In a large scale, the artificial experimental settings of the two pyrite precipitation events (Drake et al., 2015a and this study) are similar and their time scales roughly agree. However, there is one fundamental difference in the geochemical environment. At Olkiluoto, the contents of DOC in groundwater at the research site are 18–73 mg/L, whereas at Äspo the contents of DOC were much lower, ranging from 1.1 to 7.5 mg/L (Drake et al., 2015a).

Acetate is the main component of DOC at the Olkiluoto site. Bell et al. (2018) concluded that geogenic hydrogen and acetate produced by acetogenic bacteria were the sources of electrons and carbon for BSR at the site. It is therefore possible that the relatively small fractionation in BSR at the Olkiluoto research site compared to that at Äspo (Drake et al., 2015a) could be related to the specific conditions of BSR, fueled by geogenic hydrogen in the presence of abundant acetate.

6. Conclusions

We investigated mineral precipitation on the surface of drillcore equipment at a depth of 530 mbsl in crystalline bedrock at Olkiluoto, western Finland. Precipitated mineral material offered the possibility to investigate the concentrations of selected redox sensitive elements, the isotopic composition of carbon and oxygen in calcite and the isotopic composition of sulfur in pyrite. The analytical data led to the following conclusions:

- The geochemical characteristics of the groundwater system at the investigation site deviate significantly from the natural baseline conditions. The new data from the precipitated material are compatible with earlier conclusions that drilling and tunneling operations have caused inflow of water from the overlying sulfate-bearing groundwater units.
- Based on carbon and oxygen isotope ratios, calcite has precipitated in near isotopic equilibrium with its groundwater environment.
- The dissolution of old fracture filling calcite is a potential source of carbon for the new calcite precipitate. Despite the high contents of methane and acetate in the system, the carbon isotope ratios of calcite do not provide any evidence of active methane or acetate-related microbial processes in the precipitation environment.
- The fractionation of sulfur between dissolved sulfate and pyrite is inferred to be 25 ± 10‰. This is in agreement with the results reported in laboratory experiments for BSR.

Declaration of competing interest

The authors declare that they have no known competing financial interests or personal relationships that could have appeared to influence the work reported in this paper.

Acknowledgements

This study was funded by Posiva Oy and the Vilho, Yrjö and Kalle Väisälä Foundation of the Finnish Academy of Science and Letters. We thank Juhani Virkanen for ICP-MS analysis, Radoslaw Michallik for helping with EPMA, and Kerstin Lindén for sample preparation at the Nordsim laboratory. We wish to thank the anonymous reviewers, whose critical comments and suggestions helped to improve the manuscript. This is publication #710 of NordSIMS. The NordSIMS facility was supported by Swedish Research Council infrastructure grant 2017-00671 at the time of analysis. This is publication #0008 of the Geophysical, Environmental and Minerological laboratories (Hellabs) of the Department of Geosciences and Geography, University of Helsinki.

APPENDIX 1. EPMA results of calcite in the precipitate

OL-KR46_570.5								
Depth (mbsl)	Label	C (w%)	O (w%)	Mg (w%)	Ca (w%)	Mn (w%)	Fe (w%)	Zn (w%)
530	p1	16.44	44.50	0.65	37.46	0.91	0.03	0.01
530	p2	16.36	44.28	0.57	37.70	1.09	0.00	0.00
530	p3	16.37	44.30	0.66	37.80	0.88	0.00	0.00
530	p4	16.43	44.34	0.53	37.88	0.76	0.05	0.01
530	p5	16.41	44.44	0.62	37.45	1.01	0.08	0.00
530	p6	16.75	45.30	0.60	36.38	0.93	0.03	0.02
530	p7	16.39	44.47	0.65	37.23	0.87	0.33	0.06
530	p8	16.39	44.33	0.61	37.74	0.87	0.05	0.00
530	p9	16.64	44.93	0.55	37.03	0.76	0.08	0.00
530	p10	16.72	45.12	0.50	36.76	0.86	0.04	0.00

APPENDIX 2. $\delta^{34}S$ values of pyrite, and $\delta^{13}C$ and $\delta^{18}O$ values of calcite

Drillhole	Depth (mbsl)	Sample ID	$\delta^{34}S$ (VCDT)	$\delta^{18}O$ (VPDB)	$\delta^{13}C$ (VPDB)
OL-KR46_570.5	530	G4-1		−7.41	−10.19
		G4-2		−9.09	−10.39
		G4-3		−7.95	−10.32
		G6-1	2.83	−8.36	−9.90
		G6-2		−7.58	−12.07
		G6-3	4.72	−8.17	−10.32
		G15-1	8.34	−7.81	−11.20
		G15-2	−0.89	−7.72	−13.17
		G15-3	−5.71	−7.96	
		G16-1		−7.51	−10.35
		G16-2		−8.83	−10.35
		G16-3		−7.76	−9.73
		G18-1	2.92		
		G18-2	2.86		
		G18-3	−0.80		
		G18-4	−0.44		
		G19-4		−8.36	−10.13
		G19-2		−7.67	
		G19-3		−8.18	−12.27

APPENDIX 3. SIMS run data for sulfur in pyrite and carbon and oxygen in calcite

SIMS run data for sulfur in pyrite and carbon and oxygen in calcite.

Chosen std	**S0302A pyrite**
$\delta^{34}S$ (std, ‰)	**0.00**
extl. error (‰, 1SD)	**0.06**
drift corr (‰/run)	**0 (no drift corr. (default))**

average	**0.389**
SD	**0.006**
ref.	**0.002005**

Sample	Seq. in	^{32}S cps	$^{32}S_{samp/av.std}$	$^{34}S/^{32}S$	± abs	$\delta^{34}S$	± ‰	$\delta^{34}S$	± ‰	Stage position (µm)		Field ap. (digits)			IMF (%)
ID	run	(x 10^9)		*drift corrected*		*samples*		*standards*		x	y	x	y		standards
S0302A_S_mt1726_@1	1	1.08		0.04433592	0.00000240			0.03	0.08	-5216	497	11	-7	< 0.01	0.392
S0302A_S_mt1726_@2	2	1.10		0.04433009	0.00000120			-0.10	0.06	-5266	497	10	-8	< 0.01	0.379
S0302A_S_mt1726_@3	3	1.10		0.04433611	0.00000159			0.04	0.07	-5316	497	9	-8	< 0.01	0.393
S0302A_S_mt1726_@4	4	1.09		0.04433307	0.00000126			-0.03	0.06	-5366	497	10	-8	< 0.01	0.386
G15_mt1726_S	8	0.10	0.10	0.04470424	0.00000760	8.34	0.18			3453	1737	26	-7	< 0.01	
G15_mt1726_S@1	10	0.12	0.11	0.04429483	0.00000975	-0.89	0.23			3500	1774	32	-7	< 0.01	
S0302A_S_mt1726_@5	11	1.08		0.04433097	0.00000092			-0.08	0.06	-5416	497	10	-8	< 0.01	0.381
S0302A_S_mt1726_@6	12	1.08		0.04433486	0.00000100			0.01	0.06	-5466	497	10	-8	< 0.01	0.390
G15_mt1726_S@3	14	0.14	0.13	0.04408129	0.00001408	-5.71	0.32			3409	2143	27	-6	< 0.01	
G6_mt1726_S@0	16	0.11	0.10	0.04445992	0.00000756	2.83	0.18			-1050	-2514	12	-11	< 0.01	
G6_mt1726_S@1	17	0.15	0.14	0.04454364	0.00000895	4.72	0.21			-976	-2442	18	-9	< 0.01	
G18_mt1726_S	18	0.12	0.11	0.04446390	0.00000572	2.92	0.14			3866	-423	25	-8	< 0.01	
S0302A_S_mt1726_@7	19	1.07		0.04433844	0.00000143			0.09	0.07	-5516	497	10	-8	< 0.01	0.398
S0302A_S_mt1726_@8	20	1.07		0.04433607	0.00000109			0.04	0.06	-5216	447	11	-8	< 0.01	0.393
G18_mt1726_S@0	21	0.19	0.17	0.04446099	0.00000361	2.86	0.10			4000	-461	26	-9	< 0.01	
G18_mt1726_S@2	23	0.11	0.10	0.04429885	0.00000642	-0.80	0.16			3955	-548	24	-8	< 0.01	
G18_mt1726_S@4	25	0.15	0.14	0.04431508	0.00000496	-0.44	0.13			3982	-554	29	-8	< 0.01	
S0302A_S_mt1726_@9	26	1.06		0.04433641	0.00000128			0.05	0.06	-5266	447	10	-8	< 0.01	0.394
S0302A_S_mt1726_@10	27	1.06		0.04433128	0.00000092			-0.07	0.06	-5316	447	10	-8	< 0.01	0.382
S0302A_S_mt1726_@11	33	1.06		0.04433402	0.00000093			-0.01	0.06	-5366	447	10	-9	< 0.01	0.388
S0302A_S_mt1726_@12	34	1.06		0.04433544	0.00000118			0.02	0.06	-5416	447	10	-9	< 0.01	0.391

Chosen std	**S0161 cc**
$\delta^{13}C$ (std, ‰)	**0.22**
extl. error (‰, 1SD)	**0.30**
drift corr (‰/run)	**0 (no drift corr. (default))**

average	**-2.228**
SD	**0.029**
ref.	**0.002005**

Sample	Seq. in	^{12}C cps	$^{12}C_{samp/av.std}$	$^{13}C/^{12}C$	± abs	$\delta^{13}C$	± ‰	$\delta^{13}C$	± ‰	Stage position (µm)		Field ap. (digits)			IMF (%)
ID	run	(x 10^9)		*drift corrected*		*samples*		*standards*		x	y	x	y		standards
S0161_C_mt1726_@1	1	0.02		0.01093507	0.00000269			0.42	0.39	-4828	3240	-13	-7	< 0.01	-2.208
S0161_C_mt1726_@2	2	0.02		0.01093703	0.00000236			0.60	0.37	-4820	2917	-12	-9	< 0.01	-2.191
S0161_C_mt1726_@3	3	0.02		0.01092726	0.00000235			-0.29	0.37	-4906	2968	-13	-10	< 0.01	-2.278
G4_mt1726_C	4	0.02	0.97	0.01081914	0.00000284	-10.19	0.39			197	18	1	-9	< 0.01	
G4_mt1726_C@0	5	0.02	0.99	0.01081691	0.00000235	-10.39	0.37			195	-81	0	-9	< 0.01	
G4_mt1726_C@1	6	0.02	0.97	0.01081765	0.00000237	-10.32	0.37			-293	8	-2	-11	< 0.01	
G6_mt1726_C	7	0.02	1.03	0.01079853	0.00000230	-12.07	0.36			-1030	-1965	-5	-14	< 0.01	
G6_mt1726_C@0	8	0.02	0.98	0.01081771	0.00000243	-10.32	0.37			-961	-2793	-3	-13	< 0.01	
S0161_C_mt1726_@4	9	0.02		0.01093143	0.00000338			0.09	0.43	-4908	2917	-13	-9	< 0.01	-2.241
S0161_C_mt1726_@5	10	0.02		0.01093095	0.00000236			0.04	0.37	-4954	2864	-13	-9	< 0.01	-2.245
G6_mt1726_C@1	11	0.02	0.99	0.01082227	0.00000250	-9.90	0.37			-1375	-2804	-3	-14	< 0.01	
G19_mt1726_C	12	0.02	0.97	0.01081979	0.00000240	-10.13	0.37			2300	-2221	3	-14	< 0.01	
G19_mt1726_C@0	13	0.04	2.01	0.01043483	0.00000225	cps limit				2704	-2232	5	-17	< 0.01	
G19_mt1726_C@1	14	0.02	1.04	0.01079630	0.00000230	-12.27	0.36			2292	-2721	5	-15	< 0.01	
G15_mt1726_C	15	0.02	1.03	0.01080801	0.00000232	-11.20	0.36			3060	1956	6	-9	< 0.01	
S0161_C_mt1726_@6	16	0.02		0.01093336	0.00000259			0.26	0.38	-5033	2868	-14	-10	< 0.01	-2.224
G15_mt1726_C@0	17	0.02	1.07	0.01078648	0.00000262	-13.17	0.38			3217	1703	5	-11	< 0.01	
G15_mt1726_C@1	18	0.02	0.81	0.01081260	0.00000260	cps limit				3714	2186	3	-11	< 0.01	
G16_mt1726_C	19	0.02	1.04	0.01081732	0.00000275	-10.35	0.39			5331	1436	9	-11	< 0.01	
G16_mt1726_C@0	20	0.02	0.97	0.01081730	0.00000240	-10.35	0.37			5203	1752	10	-12	< 0.01	
G16_mt1726_C@1	21	0.02	0.93	0.01082415	0.00000270	-9.73	0.39			5053	1334	8	-12	< 0.01	
S0161_C_mt1726_@7	22	0.02		0.01093503	0.00000269			0.42	0.39	-5101	2887	-15	-11	< 0.01	-2.209

Chosen std	S0161 cc (PDB)		
$\delta^{18}O$ (std, ‰)	-5.62	average	3.013
extl. error (‰, 1SD)	0.14	SD	0.015
drift corr (‰/run)	0.028 (linear)		
		ref.	0.002005

Sample	Seq. in	^{16}O cps	$^{16}O_{samp/av.std}$	$^{18}O/^{16}O$	± abs	$\delta^{18}O$	± ‰	$\delta^{18}O$	± ‰	Stage position (µm)		Field ap. (digits)			IMF (%)
ID	run	(x 10^9)		drift corrected		samples		standards		x	y	x	y		standards
S0161_O_mt1726_@1	1	3.21		0.00205410	0.00000012			-5.57	0.16	-5015	1484	-7	-10	< 0.01	3.018
S0161_O_mt1726_@2	2	3.20		0.00205408	0.00000012			-5.58	0.16	-5065	1484	-11	-11	< 0.01	3.017
S0161_O_mt1726_@3	3	3.19		0.00205380	0.00000014			-5.72	0.16	-5115	1484	-9	-12	< 0.01	3.003
S0161_O_mt1726_@4	4	3.18		0.00205423	0.00000015			-5.51	0.16	-5165	1484	-8	-11	< 0.01	3.024
G4_mt1726_ox	5	3.34	1.05	0.00205030	0.00000015	-7.41	0.16			-592	328	-7	-10	< 0.01	
G4_mt1726_ox@0	6	3.31	1.04	0.00204683	0.00000019	-9.09	0.17			-619	261	-10	-4	< 0.01	
G4_mt1726_ox@1	7	3.37	1.06	0.00204920	0.00000014	-7.95	0.16			-1053	21	-11	-9	< 0.01	
G6_mt1726_ox	8	3.27	1.03	0.00204834	0.00000013	-8.36	0.16			121	-2558	-11	-13	< 0.01	
G6_mt1726_ox@0	9	3.37	1.06	0.00204996	0.00000012	-7.58	0.15			-311	-2844	-15	-16	< 0.01	
S0161_O_mt1726_@5	10	3.17		0.00205375	0.00000019			-5.75	0.17	-5215	1484	-12	-12	< 0.01	3.000
S0161_O_mt1726_@6	11	3.16		0.00205411	0.00000016			-5.57	0.16	-5265	1484	-13	-12	< 0.01	3.018
G6_mt1726_ox@1	12	3.37	1.07	0.00204875	0.00000020	-8.17	0.17			-510	-1974	-16	-14	< 0.01	
G19_mt1726_ox	13	3.21	1.02	0.00204835	0.00000016	-8.36	0.16			2656	-621	-11	-11	< 0.01	
G19_mt1726_ox@0	14	3.30	1.05	0.00204978	0.00000020	-7.67	0.17			2377	-143	-11	-7	< 0.01	
G19_mt1726_ox@1	15	3.27	1.03	0.00204871	0.00000018	-8.18	0.17			2673	43	-17	-10	< 0.01	
G15_mt1726_ox	16	3.33	1.05	0.00204949	0.00000012	-7.81	0.15			497	3548	-5	-3	< 0.01	
S0161_O_mt1726_@7	17	3.15		0.00205341	0.00000015			-5.91	0.16	-5315	1484	-13	-13	< 0.01	2.983
S0161_O_mt1726_@8	18	3.17		0.00205442	0.00000021			-5.42	0.17	-5115	1434	-11	-8	< 0.01	3.034
G15_mt1726_ox@0	19	3.32	1.05	0.00204966	0.00000016	-7.72	0.16			867	3636	-5	-6	< 0.01	
G15_mt1726_ox@1	20	3.32	1.05	0.00204917	0.00000014	-7.96	0.16			1144	3975	-1	-6	< 0.01	
G16_mt1726_ox	21	3.18	1.00	0.00205009	0.00000014	-7.51	0.16			2583	4129	0	-6	< 0.01	
G16_mt1726_ox@0	22	3.22	1.02	0.00204737	0.00000019	-8.83	0.17			2629	4193	0	-5	< 0.01	
G16_mt1726_ox@1	23	3.12	0.99	0.00204959	0.00000020	-7.76	0.17			2702	4592	2	-2	< 0.01	
S0161_O_mt1726_@9	24	3.13		0.00205424	0.00000015			-5.51	0.16	-5165	1434	-12	-10	< 0.01	3.025
S0161_O_mt1726_@10	25	3.16		0.00205393	0.00000022			-5.66	0.18	-5215	1434	-12	-10	< 0.01	3.009

. (*continued*).

References

Aaltonen, I., Engström, J., Front, K., Gehör, S., Kosunen, P., Kärki, A., Paananen, M., Paulamäki, S., Mattila, J., 2016. Geology of Olkiluoto. Posiva Report 2016-16, ed., p. 398 Posiva Oy, Olkiluoto, Finland.

Allard, B., Larsson, S.Å., Tullborg, E.-L., Wikberg, P., 1983. Chemistry of Deep Groundwaters from Granitic Bedrock. SKBF/KBS Technical Report 83-59.

Bell, E., Lamminmäki, T., Alneberg, J., Andersson, A.F., Qian, C., Xiong, W., Hettich, R. L., Balmer, L., Frutschi, M., Sommer, G., Bernier-Latmani, R., 2018. Biogeochemical cycling by a low-diversity microbial community in deep groundwater. Front. Microbiol. 9, 2129.

Bell, E., Lamminmäki, T., Pitkänen, P., Bernier-Latmani, R., 2020. Microbial Metabolism Resulting from the Mixing of Sulfate-Rich and Methane-Rich Deep Olkiluoto Groundwaters in Drillholes OL-KR11, OL-KR13 and OL-KR46. Posiva Working Report 2020-02 (Posiva Oy, Olkiluoto, Finland).

Blaser, M.B., Dreisbach, L.K., Conrad, R., 2013. Carbon isotope fractionation of 11 acetogenic strains grown on H_2 and CO_2. Appl. Environ. Microbiol. 79, 1787–1794.

Blyth, A., Frape, S., Blomqvist, R., Nissinen, P., 2000. Assessing the past thermal and chemical history of fluids in crystalline rock by combining fluid inclusion and isotopic investigations of fracture calcite. Appl. Geochem. 15, 1417–1437.

Blyth, A., Frape, S., Ruskeeniemi, T., Blomqvist, R., 2004. Origins, closed system formation and preservation of calcites in glaciated crystalline bedrock: evidence from Palmottu natural analogue site, Finland. Appl. Geochem. 19, 675–686.

Blyth, A., Frape, S., Tullborg, E.-L., 2009. A review and comparison of fracture mineral investigations and their application to radioactive waste disposal. Appl. Geochem. 24, 821–835.

Björk, S., 2008. The late Quaternary development of the Baltic Sea basin. In: The BACC Author Team (Ed.), Assessment of Climate Change for the Baltic Sea Basin. Springer-Verlag, Berlin Heidelberg, pp. 398–407.

Canfield, D.E., Farquhar, J., Zerkle, A.L., 2010. High isotope fractionations during sulfate reduction in a low-sulfate euxinic ocean analog. Geology 38, 415–418.

Canfield, D.E., 2001. Biochemistry of sulfur isotopes. In: Valley, J.W., Cole, D.R. (Eds.), Reviews in Mineralogy and Geochemistry 43, Stable Isotope Geochemistry. Mineralogical Society of America, pp. 607–636.

Canfield, D.E., Thamdrup, D., 1994. The production of 34S-depleted sulfide during bacterial disproportionation of elemental sulfur. Science 266, 1973–1975.

Chambers, L.A., Trudinger, P.A., 1979. Microbial fractionation of stable sulfur isotopes: a review and critique. Geomicrobiology 1, 249–293.

Detmers, J., Brüchert, V., Habicht, K.S., Kuever, J., 2001. Diversity of sulfur isotope fractionation by sulfate reducing prokaryotes. Appl. Environ. Microbiol. 67, 888–894.

Drake, H., Tullborg, E.-L., 2009. Paleohydrogeological events recorded by stable isotopes, fluid inclusions and trace elements in fracture minerals in crystalline rock, Simpevarp area, SE Sweden. Appl. Geochem. 24, 715–732.

Drake, H., Tullborg, E.-L., Page, L., 2009. Distinguished multiple events of fracture mineralisation related to far-field orogenic effects in Paleoproterozoic crystalline rocks, Simpevarp area, SE Sweden. Lithos 110, 37–49.

Drake, H., Tullborg, E.-L., Hogmalm, J., Åström, M., 2012. Trace metal distribution and isotope variations in low-temperature calcite and groundwater in granitoid fractures down to 1 km depth. Geochem. Cosmochim. Acta 84, 217–238.

Drake, H., Åström, M., Tullborg, E.-L., Whitehouse, M., Fallick, A.E., 2013. Variability of sulphur isotope ratios in pyrite and dissolved sulphate in granitoid fractures down to 1 km depth - evidence of widespread activity of sulphur reducing bacteria. Geochem. Cosmochim. Acta 102, 143–161.

Drake, H., Tullborg, E.-L., Whitehouse, M., Sandberg, B., Blomfeldt, T., Åström, M., 2015a. Extreme fractionation and micro-scale variation of sulphur isotopes during bacterial sulphate reduction in deep groundwater systems. Geochem. Cosmochim. Acta 161, 1–18.

Drake, H., Åström, M.E., Heim, C., Broman, C., Åström, J., Whitehouse, M.J., Ivarsson, M., Siljeström, S., Sjövall, P., 2015b. Extreme 13C-depletion of carbonates formed during oxidation of biogenic methane in fractured granite. Nat. Commun. 6, 7020.

Drake, H., Heim, C., Roberts, N., Zack, T., Tillberg, M., Broman, C., Ivarsson, M., Whitehouse, M., Åström, M., 2017. Isotopic evidence for microbial production and consumption of methane in the upper continental crust throughout the Phanerozoic eon. Earth Planet Sci. Lett. 470, 108–118.

Drake, H., Mathurin, F., Zack, T., Schäfer, T., Roberts, N., Whitehouse, M., Karlsson, A., Broman, C., Åström, M., 2018a. Incorporation of metals into calcite in a deep anoxic granite aquifer. Environ. Sci. Technol. 52, 493–502.

Drake, H., Ivarsson, M., Tillberg, M., Whitehouse, M., Kooijman, E., 2018b. Ancient microbial activity in deep hydraulically conductive fracture zones within the forsmark target area for geological nuclear waste disposal, Sweden. Geosciences 8, 211.

Drake, H., Whitehouse, M., Heim, C., Reiners, P., Tillberg, M., Hogmalm, K.J., Dopson, M., Broman, C., Åström, M., 2018c. Unprecedented 34S-enrichment of pyrite formed following microbial sulfate reduction in fractured crystalline rocks. Geobiology 16, 556–574.

Gomes, M., Hurtgen, M., 2013. Sulfur isotope systematics of a euxinic, low-sulfate lake: evaluating the importance of the reservoir effect in modern and ancient oceans. Geology 41, 663–666.

Gehör, S., Karhu, J., Kärki, A., Löfman, J., Pitkänen, P., Ruotsalainen, P., Taikina-aho, O., 2002. Fracture Calcites at Olkiluoto. Posiva Report 2002-03, p. 118. Posiva Oy, Olkiluoto, Finland.

Habicht, K.S., Canfield, D., 1997. Sulfur isotope fractionation during bacterial sulfate reduction in organic-rich sediments. Geochem. Cosmochim. Acta 61, 5351–5361.

Habicht, K.S., Canfield, D., Rethmeier, J., 1998. Sulfur isotope fractionation during bacterial reduction and disproportionation of thiosulfate and sulfite. Geochem. Cosmochim. Acta 62, 2585–2595.

Habicht, K.S., Canfield, D., 2001. Isotope fractionation by sulfate reducing natural populations and the isotopic composition of sulfide in marine sediments. Geology 29, 555–558.
Habicht, K.S., Gade, M., Thamdrup, B., Berg, P., Canfield, D., 2002. Calibration of sulfate levels in the Archean ocean. Science 298, 2372–2374.
Hallbeck, L., Pedersen, K., 2008. Characterization of microbial processes in deep aquifers of the Fennoscandian Shield. Appl. Geochem. 23, 1796–1819.
Harrison, A.G., Thode, H.G., 1958. Mechanics of the bacterial reduction of sulfate from isotope fractionation studies. Trans. Faraday Soc. 53, 84–92.
Iwatsuki, T., Satake, H., Metcalfe, R., Yoshida, H., Kama, K., 2002. Isotopic and morphological features of fracture calcite from granitic rocks of the tono area, Japan: a promising palaeohydrogeological tool. Appl. Geochem. 17, 1241.
Johnston, D.T., Farquhar, J., Canfield, D.E., 2007. Sulfur isotope insights into microbial sulfate reduction: when microbes meet models. Geochem. Cosmochim. Acta 71, 3929–3947.
Kamber, B.S., Whitehouse, M.J., 2007. Micro-scale sulphur isotope evidence for sulphur cycling in the late Archean shallow ocean. Geobiology 5, 5–17.
Kaplan, I.R., Rittenberg, S.C., 1964. Microbiological fractionation of sulphur isotopes. J. Gen. Microbiol. 34, 195–212.
Kraal, P., Burton, E.D., Bush, R.T., 2013. Iron monosulfide accumulation and pyrite formation in eutrophic estuarine sediments. Geochem. Cosmochim. Acta 122, 75–88.
Kärki, A., Paulamäki, S., 2006. Petrology of Olkiluoto. Posiva Report 2006-02, p. 77. Posiva Oy, Olkiluoto, Finland.
Laaksoharju, M., Smellie, J., Tullborg, E.-L., Gimeno, J., Molinero, I., Gurban, I., Hallbeck, L., 2008. Hydrogeochemical evaluation and modelling performed within the Swedish site investigation programme. Appl. Geochem. 23, 1761–1795.
Lamminmäki, T., Pitkänen, P., Penttinen, T., Loimula, K., Partamies, S., Ahokas, T., 2017. Results of Monitoring at Olkiluoto in 2013, Hydrogeochemistry. Posiva Working Report 2014-44 (Posiva Oy, Olkiluoto, Finland).
Lamminmäki, T., Pitkänen, P., Penttinen, T., Komulainen, J., Loimula, K., Wendling, L., Partamies, S. and Ahokas, T. Results of Monitoring at Olkiluoto in 2014, Hydrogeochemistry. Posiva Working Report 2015-44, (Posiva Oy, Olkiluoto, Finland).
Lamminmäki, T., Pitkänen, P., Penttinen, T., Pentti, E., Komulainen, J., Loimula, K., Wendling, L., Partamies, S. and Ahokas, T. Results of Monitoring at Olkiluoto in 2015, Hydrogeochemistry. Posiva Working Report 2016-44, (Posiva Oy, Olkiluoto, Finland).
Morse, J.W., Millero, F.J., Cornwell, J.C., Rickard, D., 1987. Chemistry of the hydrogen sulphide and iron sulphide systems in natural waters. Earth Sci. Rev. 24, 1–42.
O'Neil, J.R., Clayton, R.N., Mayeda, T.K., 1969. Oxygen isotope fractionation in divalent metal carbonates. J. Chem. Phys. 51, 5547–5558.
Pedersen, K., Arlinger, J., Hallbeck, A., Hallbeck, L., Eriksson, S., Johansson, J., 2008. Numbers, biomass and cultivable diversity of microbial populations related to depth and borehole-specific conditions in groundwater from depths of 4 to 450 m in Olkiluoto, Finland. ISME J. 2, 760–775.
Pitkänen, P., Partamies, S., Luukkonen, A., 2004. Hydrogeochemical Interpretation of Baseline Groundwater Conditions at the Olkiluoto Site. Posiva Report 2003-07, p. 159. Posiva Oy, Olkiluoto, Finland.
Posiva, 2013. Olkiluoto Site Description 2011. Posiva Report 2011-2. Posiva Oy, p. 1029. Posiva Oy, Olkiluoto, Finland.
Rickard, D., 1997. Kinetics of pyrite formation by the H2S oxidation of iron (II) monosulfide in aqueous solutions between 25 and 125 °C: the rate equation. Geochem. Cosmochim. Acta 61, 115–134.
Rickard, D., Luther, G.W., 2007. Chemistry of iron sulfides. Chem. Rev. 107, 514–562.
Romanek, C.S., Grossman, E.L., Morse, J.W., 1992. Carbon isotope fractionation in synthetic aragonite and calcite: effects of temperature and precipitation rate. Chem. Iron Sulf. 56, 419–430.
Sahlstedt, E., Karhu, J.A., 2016. Fracture mineral Investigations from Fissure Fillings with Emphasis on the Eastern Side of the Olkiluoto Island: a Repost of Investigations in 2012. Posiva Working Report 2016-33. Posiva Oy.
Sahlstedt, E., Karhu, J.A., Pitkänen, P., 2010. Indications for the past redox environments in deep groundwaters from the isotopic composition of carbon and oxygen in fracture calcite, Olkiluoto, SW Finland. Isot. Environ. Health Stud. 46, 370–391.
Sahlstedt, E., Karhu, J.A., Pitkänen, P., Whitehouse, M., 2013. Implications of sulfur isotope fractionation in fracture-filling sulfides in crystalline bedrock, Olkiluoto, Finland. Appl. Geochem. 32, 52–69.
Sahlstedt, E., Karhu, J.A., Pitkänen, P., Whitehouse, M., 2016. Biogenic processes in crystalline bedrock fractures indicated by carbon isotope signatures of secondary calcite. Appl. Geochem. 67, 30–41.
Schoonen, M.A.A., Barnes, H.L., 1991. Reactions forming pyrite and marcasite from solution: II. Via FeS precursors below 100 °C. Geochem. Cosmochim. Acta 55, 1505–1514.
Sim, M.S., Bosak, T., Ono, S., 2011. Large isotope fractionation does not require disproportionation. Science 333, 74–77.
Smellie, J., Pitkänen, P., Koskinen, L., Aaltonen, I., Eichinger, F., Waber, N., Sahlstedt, E., Siitari-Kauppi, M., Karhu, J., Löfman, J., Poteri, A., 2014. Evolution of the Olkiluoto Site: Palaeohydrogeochemical Considerations, Posiva Working Report 2014-27 (Posiva Oy, Olkiluoto, Finland).
Suominen, V., Fagerström, P., Torssonen, M., 1997. Pre-Quaternary rocks of the Rauma map-sheet area (in Finnish with an English summary). In: Geological Survey of Finland, Geological Map of Finland 1:100 000, Explanation to the maps of Pre-Quaternary rocks, Sheet, 1132, p. 54.
Tullborg, E.-L., Landström, O., Wallin, B., 1999. Low-temperature trace element mobility influenced by microbial activity: indications from fracture calcite and pyrite in crystalline basement. Chem. Geol. 157, 199–218.
Tullborg, E.-L., Drake, H., Sandstörm, B., 2008. Paleohydrogeology: a methodology based on fracture mineral studies. Appl. Geochem. 23, 1881–1897.
Tuomi, P., Lamminmäki, T., Pedersen, K., Miettinen, H., Bomberg, M., Bell, E., Bernier-Latmani, R., Pitkänen, P., 2020. Conceptual Model of Microbial Effects on Hydrogeochemical Conditions at the Olkiluoto Site, Posiva Report 2020-03, p. 278. Posiva Oy, Olkiluoto, Finland.
Veräjämäki, A., 1998. Pre-Quaternary rocks of the Kokemäki map-sheet area (in Finnish with an English summary). In: Geological Survey of Finland, Geological Map of Finland 1:100 000, Explanation to the maps of Pre-Quaternary rocks, Sheet, 1134, p. 51.
Wilkin, R.T., Barnes, H.L., 1996. Pyrite formation by reactions of iron monosulfides with dissolved inorganic and organic sulfur species. Geochem. Cosmochim. Acta 60, 4167–4179.
Wortmann, U.G., Bernasconi, S.M., Böttcher, M.E., 2001. Hypersulfidic deep biosphere indicates extreme sulfur isotope fractionation during single-step microbial sulfate reduction. Geology 29, 647–650.
Zaback, D.A., Pratt, L.M., Hayes, J.M., 1993. Transport and reduction of sulfate and immobilization of sulfide in marine black shale. Geology 21, 141–144.
Zhang, J., Quau, P.D., Wilbur, D.O., 1995. Carbon isotope fractionation during gas-water exchange and dissolution of CO_2. Geochem. Cosmochim. Acta 59, 107–114.